ARTICLE

Collisional Line Assignments and Hyperfine Structure Interpretation in Cs_2 $2^3\Delta_{1g}$ State

Dan Li[a], Feng Xie[b*], Li Li[c], Ergin H. Ahmed[d], A. Marjatta Lyyra[d]

a. Center for Photonics and Electronics, State Key Laboratory of Tribology, Department of Precision Instruments and Mechanology, Tsinghua University, Beijing 100084, China
b. Institute of Nuclear and New Energy Technology, Tsinghua University, Beijing 100084, China
c. Department of Physics, Tsinghua University, Beijing 100084, China
d. Department of Physics, Temple University, Philadelphia, Pennsylvania 19122-6082, USA

(Dated: Received on December 14, 2012; Accepted on January 14, 2013)

Accurately known energy level structure of the Cs_2 $A^1\Sigma_u^+$-$b^3\Pi_u$ complex of states from a recent global de-perturbation of these states has enabled additional assignments of 140 perturbation facilitated infrared-infrared double resonance (PFIIDR) transitions to the $2^3\Delta_{1g}$ state from collisionally populated intermediate $A^1\Sigma_u^+$ levels. Together with the 221 previously observed $2^3\Delta_{1g}\leftarrow A^1\Sigma_u^+\leftarrow X^1\Sigma_g^+$ double resonance lines [J. Chem. Phys. **128**, 204313 (2008)], molecular constants and the Rydberg-Klein-Rees potential energy curve of the $2^3\Delta_{1g}$ state have been recalculated (excluding 54 perturbed levels). The centrifugal distortion constant has been determined and agrees well with the value calculated based on standard empirical formulas. The hyperfine structure of the $2^3\Delta_g$ state, which has not resolved in our sub-Doppler excitation spectra of the $2^3\Delta_{1g}$ state, has been interpreted with a preliminary simulation.

Key words: Cs_2, $2^3\Delta_{1g}$ state, Collision-induced energy transfer, Hyperfine structure

I. INTRODUCTION

The cesium dimer Cs_2 has attracted much attention for its important role in both fundamental and applied research, including laser cooling of molecules, coherent control *etc.* The ground state, $X^1\Sigma_g^+$, has been studied by Fourier transform spectroscopy and accurate molecular constants have been reported [1]. Later, a direct potential fitting procedure has been performed to the $X^1\Sigma_g^+\leftarrow A^1\Sigma_u^+$ transitions in Cs_2 to generate the first fully analytical potential energy function for the $X^1\Sigma_g^+$ state [2]. Recently, a global analysis of experimental data on the spin-orbit-coupled $A^1\Sigma_u^+$ and $b^3\Pi_u$ states of Cs_2 has been completed and highly accurate term values of these intermediate states are now available [3]. The $A^1\Sigma_u^+$-$b^3\Pi_u$ mixed levels have been used as gateway or "window" states for the excitation of higher triplet states [4−8].

In our earlier work [6], based on 221 observed $2^3\Delta_{1g}\leftarrow A^1\Sigma_u^+\leftarrow X^1\Sigma_g^+$ double resonance lines, molecular constants and the Rydberg-Klein-Rees (RKR) potential curve were reported for the $2^3\Delta_{1g}$ state. In the report by Xie *et al.* the weak features around the perturbation facilitated optical-optical double resonance excitation lines were considered to be hyperfine structures [6]. Careful analysis indicates that these weak features were not hyperfine lines but collisional satellite lines.

In this work, collisional line assignments are presented. Molecular constants and the RKR potential energy curve of the $2^3\Delta_{1g}$ state are recalculated. The hyperfine structure in the $2^3\Delta_{1g}$ state, as well as in $2^3\Delta_{2g}$ and $2^3\Delta_{3g}$ states, is interpreted with a preliminary simulation.

II. EXPERIMENTS

The experimental setup is similar to that used in our previous Cs_2 and K_2 infrared-infrared double resonance experiment [4−11]. Here a brief description about the experiment is given. Cesium vapor was generated in a heatpipe oven with 1 Torr Ar buffer gas. The vapor temperature was about 300 °C. A single mode tunable DL100 diode laser (9620−9830 cm^{-1} scanning range, ∼25 mW power at the entrance window of the oven, 5 MHz linewidth) was used as the pump laser to excite the $A^1\Sigma_u^+\leftarrow X^1\Sigma_g^+$ transitions and a CR 899-29 Titanium Sapphire probe laser (300 mW output, 1 MHz linewidth) was used as the probe laser to further excite the $2^3\Delta_{1g}\leftarrow A^1\Sigma_u^+$ transition. The two laser beams counter-propagated and crossed at the heatpipe center. Double resonance signals were detected

*Author to whom correspondence should be addressed. E-mail: fxie@mail.tsinghua.edu.cn, Tel.: +86-10-62771140, FAX: +86-10-62797135

by monitoring the $2^3\Delta_{1g}\rightarrow b^3\Pi_u$ and collision induced $^3\Pi_g/^3\Sigma_g^+\rightarrow a^3\Sigma_u^+$ fluorescence with interference filters and a photomultiplier tube.

III. RESULTS AND DISCUSSION

A. Collisonal line assignments

In homonuclear diatomic molecules, each rotational level is assigned as symmetric (s) or antisymmetric (a), depending on whether its wavefunction remains the same or changes sign upon interchanging the nuclei. This is due to a symmetry of homonuclear diatomic molecules arising from the invariance of the Hamiltonian when the two nuclei are interchanged. Collision-induced energy transfer within an electronic state and between different electronic states has been studied widely [12]. The selection rules are a↔a, s↔s, and a←/→s, which means that the allowed transitions must preserve the symmetry with respect to an interchange of the nuclei in homonuclear molecules.

The rotational levels with even J of the $A^1\Sigma_u^+$ state are antisymmetric and those with odd J are symmetric excluding the nuclear spin functions when the two nuclei are interchanged. As a result only rotational levels differing by $\Delta J=\pm2$, ±4, ±6, ..., $\pm2k$ from the parent level can be populated by collisions.

Typical excitation spectra of $2^3\Delta_{1g}\leftarrow A^1\Sigma_u^+$ in Cs_2 are shown in Fig.1. Transitions from an intermediate rotational level of the $A^1\Sigma_u^+$ state into each upper vibrational level contain P, Q, and R lines, as indicated by the strongest lines shown in the Fig.1. The weaker lines originate from excitations from collisionally populated nearby rotational levels of the $A^1\Sigma_u^+$ state into upper $2^3\Delta_{1g}$ state. Based on assignments of collisional lines in Fig.1, it is clear that the collision induced energy transfer can only occur into rotational levels differing by $\Delta J=\pm2$, ±4, ±6, ..., $\pm2k$ from the parent level in the $A^1\Sigma_u^+$ state, which is consistent with selection rules above.

In addition, the distributions of collisional lines in Fig.1 exhibit different patterns. These different patterns in the excitation spectra of the P, Q, and R branches can be interpreted with the difference of rotational constants of the intermediate $A^1\Sigma_u^+$ state ($\sim$0.00919 cm^{-1}) and upper $2^3\Delta_{1g}$ state ($\sim$0.00930 cm^{-1}).

One hundred and forty collisional lines in the excitation spectra of $2^3\Delta_{1g}\leftarrow A^1\Sigma_u^+$ in Cs_2 have been assigned based on collision-induced energy transfer rules and accurate term values of the intermediate $A^1\Sigma_u^+$ state calculated from Ref.[3]. Table I gives excitation transitions for collisional lines. We have calculated molecular constants of the $2^3\Delta_{1g}$ state including the current 140 collision-induced transitions and the earlier 221 experimentally observed $2^3\Delta_{1g}\leftarrow A^1\Sigma_u^+\leftarrow X^1\Sigma_g^+$ double resonance lines (excluding 54 perturbed levels). New Dunham constants are reported in Table II along with our earlier work and theoretical results [13]. Instead of using a fixed value for the centrifugal distortion constant D_v, which equals to $-Y_{02}$ in the fits as done in our earlier work, this constant was fitted directly using our experimental data. The new value $D_v\approx3.64\times10^{-9}$ cm^{-1} agrees well with the value, -3.52×10^{-9} cm^{-1}, calculated from the empirical formula: $-Y_{02}=4Y_{01}^3/Y_{10}^2$. The result indicates that the current molecular constants are self-consistent and cover a larger range of energy levels. The RKR potential energy curve of the $2^3\Delta_{1g}$ state has been recalculated and the values are given in Table III.

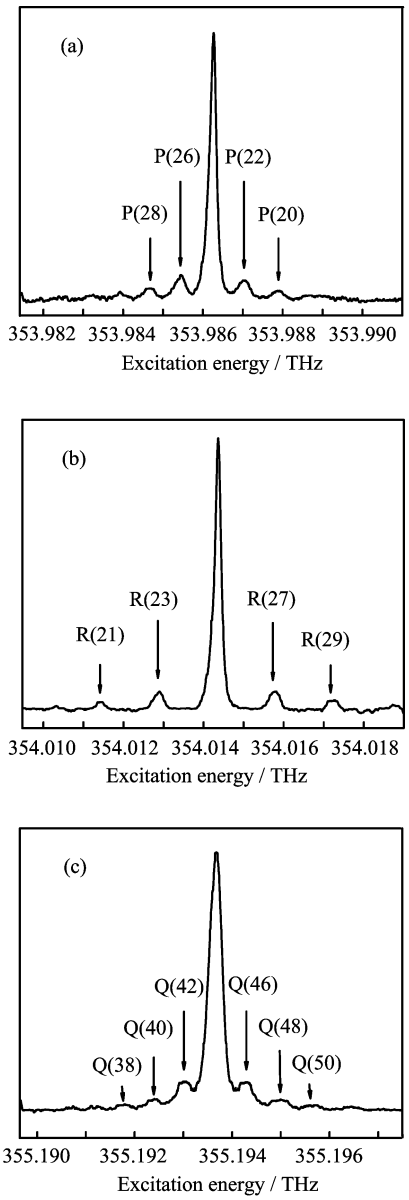

FIG. 1 Collision line assignments.
(a) $2^3\Delta_{1g}(v=8,\ J=23)\leftarrow A^1\Sigma_u^+(v'=7,\ J'=24)$ transition.
(b) $2^3\Delta_{1g}(v=8,\ J=26)\leftarrow A^1\Sigma_u^+(v'=7,\ J'=25)$ transition.
(c) $2^3\Delta_{1g}(v=8,\ J=44)\leftarrow A^1\Sigma_u^+(v'=6,\ J'=44)$ transition.

DOI:10.1063/1674-0068/26/01/13-19

TABLE I Collision line assignments of the $2^3\Delta_{1g}$ state. The term values of the intermediate state $A^1\Sigma_u^+$ is deriven from Ref.[3], unit in cm^{-1}. Frequency indicates probe laser frequency with unit in cm^{-1}.

A level		Frequency	$2^3\Delta_{1g}$ state			A level		Frequency	$2^3\Delta_{1g}$ state			A level		Frequency	$2^3\Delta_{1g}$ state		
v'	J'		Term value	v	J	v'	J'		Term value	v	J	v'	J'		Term value	v	J
6	37	11817.347	21704.607	7	37	7	28	11808.737	21730.199	8	29	6	42	11848.784	21739.708	8	43
6	39	11817.372	21706.047	7	39	7	30	11807.651	21730.200	8	29	6	42	11848.780	21739.704	8	43
6	41	11817.395	21707.558	7	41	7	28	11808.738	21730.200	8	29	6	45	11848.014	21741.362	8	45
6	41	11818.185	21708.348	7	42	7	29	11808.762	21730.758	8	30	6	45	11848.014	21741.362	8	45
6	45	11817.446	21710.794	7	45	7	31	11807.639	21730.759	8	30	6	46	11848.025	21742.217	8	46
6	45	11818.305	21711.653	7	46	7	30	11808.789	21731.338	8	31	6	46	11848.023	21742.215	8	46
6	47	11817.474	21712.544	7	47	7	30	11808.787	21731.336	8	31	6	46	11848.025	21742.217	8	46
6	49	11817.502	21714.354	7	49	7	30	11808.788	21731.337	8	31	6	45	11848.870	21742.218	8	46
6	67	11819.057	21735.257	7	68	7	31	11808.812	21731.932	8	32	6	45	11848.870	21742.218	8	46
6	67	11819.060	21735.260	7	68	6	36	11847.251	21733.831	8	35	6	46	11848.897	21743.089	8	47
6	69	11819.126	21737.845	7	70	6	36	11847.921	21734.501	8	36	6	46	11848.903	21743.095	8	47
6	69	11819.128	21737.847	7	70	6	38	11847.234	21735.192	8	37	6	46	11848.902	21743.094	8	47
6	73	11819.263	21743.250	7	74	6	37	11847.932	21735.192	8	37	6	46	11848.900	21743.092	8	47
6	73	11819.266	21743.253	7	74	6	37	11847.931	21735.191	8	37	6	46	11848.898	21743.090	8	47
6	75	11819.324	21746.067	7	76	6	38	11847.940	21735.898	8	38	6	47	11848.037	21743.107	8	47
6	75	11819.323	21746.066	7	76	6	38	11847.940	21735.898	8	38	6	47	11848.038	21743.108	8	47
7	8	11808.282	21722.921	8	9	6	38	11847.944	21735.902	8	38	6	48	11848.047	21743.999	8	48
7	10	11808.323	21723.322	8	11	6	37	11848.641	21735.901	8	38	6	48	11848.047	21743.999	8	48
7	14	11808.406	21724.326	8	15	6	37	11848.640	21735.900	8	38	6	48	11848.050	21744.002	8	48
7	18	11807.810	21724.936	8	17	6	38	11848.663	21736.621	8	39	6	47	11848.929	21743.999	8	48
7	16	11808.438	21724.932	8	17	6	38	11848.669	21736.627	8	39	6	47	11848.939	21744.009	8	48
7	19	11807.796	21725.283	8	18	6	38	11848.671	21736.629	8	39	6	48	11848.958	21744.910	8	49
7	18	11808.501	21725.638	8	19	6	40	11847.217	21736.627	8	39	6	48	11848.963	21744.915	8	49
7	18	11808.499	21725.636	8	19	6	38	11848.670	21736.628	8	39	6	48	11848.963	21744.915	8	49
7	20	11807.784	21725.624	8	19	6	39	11847.951	21736.626	8	39	6	48	11848.959	21744.911	8	49
7	18	11808.500	21725.637	8	19	6	39	11847.951	21736.626	8	39	6	48	11848.956	21744.908	8	49
7	19	11808.527	21726.014	8	20	6	40	11847.961	21737.371	8	40	6	49	11848.059	21744.911	8	49
7	21	11807.768	21726.013	8	20	6	40	11847.961	21737.371	8	40	6	49	11848.059	21744.911	8	49
7	20	11808.547	21726.387	8	21	6	40	11847.962	21737.372	8	40	6	50	11848.072	21745.842	8	50
7	20	11808.547	21726.387	8	21	6	39	11848.696	21737.371	8	40	6	50	11848.070	21745.840	8	50
7	22	11807.755	21726.385	8	21	6	39	11848.698	21737.373	8	40	6	50	11848.072	21745.842	8	50
7	20	11808.546	21726.386	8	21	6	40	11848.721	21738.131	8	41	6	49	11848.995	21745.847	8	50
7	21	11808.568	21726.813	8	22	6	40	11848.728	21738.138	8	41	6	49	11848.994	21745.846	8	50
7	23	11807.740	21726.796	8	22	6	40	11848.725	21738.135	8	41	6	50	11849.017	21746.787	8	51
7	22	11808.591	21727.221	8	23	6	42	11847.200	21738.124	8	41	6	50	11849.023	21746.793	8	51
7	22	11808.592	21727.222	8	23	6	40	11848.726	21738.136	8	41	6	50	11849.020	21746.790	8	51
7	22	11808.592	21728.149	8	23	6	40	11848.722	21738.132	8	41	6	50	11849.021	21746.791	8	51
7	23	11808.616	21727.671	8	24	6	41	11847.972	21738.135	8	41	6	52	11848.098	21747.761	8	52
7	26	11807.701	21728.149	8	25	6	41	11847.972	21738.135	8	41	7	21	11839.041	21757.286	9	22
7	27	11807.688	21728.634	8	26	6	42	11847.982	21738.906	8	42	7	23	11838.211	21757.267	9	22
7	26	11808.689	21729.137	8	27	6	42	11847.981	21738.905	8	42	7	23	11839.082	21758.138	9	24
7	26	11808.687	21729.135	8	27	6	42	11847.982	21738.906	8	42	7	23	11839.085	21758.141	9	24
7	28	11807.675	21729.137	8	27	6	41	11848.754	21738.917	8	42	7	27	11838.154	21759.100	9	26
7	26	11808.690	21729.138	8	27	6	41	11848.755	21738.918	8	42	7	27	11839.178	21760.124	9	28
7	27	11808.713	21729.659	8	28	6	42	11848.777	21739.701	8	43	7	27	11839.178	21760.124	9	28
7	29	11807.663	21729.659	8	28	6	42	11848.784	21739.708	8	43	7	29	11839.223	21761.219	9	30
7	28	11808.738	21730.200	8	29	6	42	11848.785	21739.709	8	43						

DOI:10.1063/1674-0068/26/01/13-19

TABLE II Molecular constants of the Cs_2 $2^3\Delta_{1g}$ state. All constants are in cm^{-1} except R_e, which is in Å. Y_{02} in the earlier work was computed as $-4Y_{01}^3/Y_{10}^2$.

	This work	Ref.[3]	Spies [8]
T_e+Y_{00}	21 458.406 34 (26 681)	21 451.383 43 (129 158)	21 650
Y_{10}	31.370 393 (96 177)	34.575 815 (585 528)	30.8
Y_{20}	−0.025 606 21 (1 148 533)	−0.566 117 0 (984 141)	
Y_{30}	−0.001 765 465 (454 735)	0.037 893 11 (727 646)	
Y_{40}		−0.001 066 196 (199 911)	
Y_{01}	0.009 534 811 (2 288)	0.009 539 632 (3 899)	0.009 520
Y_{11}	$-2.479\ 8\ (28\ 6)\times10^{-5}$	$-2.615\ 1\ (467)\times10^{-5}$	
Y_{02}	$-3.637\ 5\ (818)\times10^{-9}$	$-2.929\ 82\times10^{-9}$	
R_e	5.158 05 (62)	5.156 75 (105)	5.160
Y_{00}	0.007 63	−0.124 71	

TABLE III The RKR potential of the Cs_2 $2^3\Delta_{1g}$ state.

v	R_{min}/Å	R_{max}/Å	E_v/cm^{-1}	$B_v/10^{-5}cm^{-1}$
0	5.03462	5.28912	21474.0849	952.2412
1	4.94894	5.39003	21505.3983	949.7614
2	4.89215	5.46211	21536.6447	947.2816
3	4.84724	5.52233	21567.8133	944.8017
4	4.80928	5.57566	21598.8937	942.3219
5	4.77599	5.62436	21629.8752	939.8421
6	4.74611	5.66971	21660.7472	937.3623
7	4.71884	5.71251	21691.4991	934.8824
8	4.69365	5.75330	21722.1204	932.4026
9	4.67016	5.79247	21752.6004	929.9228
10	4.64807	5.83030	21782.9286	927.4429
11	4.62718	5.86704	21813.0944	924.9631
12	4.60730	5.90285	21843.0871	922.4833
13	4.58829	5.93789	21872.8962	920.0034

Figure 2 shows the current RKR potential energy curve along with that from our earlier work [6]. As indicated in Ref.[6], the vibrational energy levels v=11 and 13 are strongly perturbed, probably by the nearby $3^3\Pi_g$ state. The term values of the v=11 and 13 subsets have also been excluded from current calculations. The residuals of calculated term values using the Dunham series and the experimental $2^3\Delta_{1g}$ term are shown in Fig.3. The errors in reproducing experimental data are less than 0.025 cm^{-1} except for the vibrational levels v=11 and 13 which exhibit a strong perturbations.

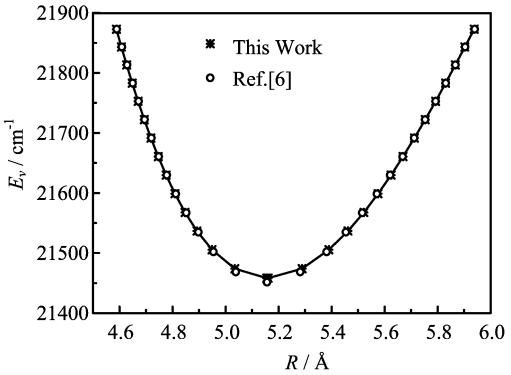

FIG. 2 The RKR potential curve of the $2^3\Delta_{1g}$ state.

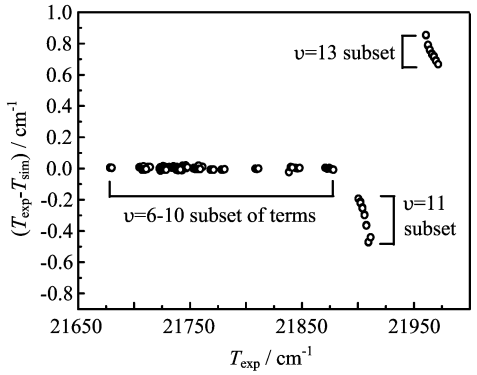

FIG. 3 Residuals of the $2^3\Delta_{1g}$ state experimental term values simulation. The perturbed vibrational levels v=11 and 13 have been excluded from the Dunham fit.

B. Hyperfine structure interpretation in the $2^3\Delta_g$ state

The Cs atom has a very large hyperfine splitting. Hyperfine splittings of several GHz in the $a^3\Sigma_u^+$ [14−16], $2^3\Pi_u$ [17], $2^3\Sigma_u^+$ [18, 19], and $3^3\Sigma_g^+$ [5] states of Cs_2 have been observed. In our $2^3\Delta_{1g}$←$A^1\Sigma_u^+$ excitation spectra, no hyperfine splitting has been resolved.

The $2^3\Delta_g$ state dissociates to the 6s+6d atomic limit, and it can be described in terms of a case (a) coupling scheme in the range of our observation [6]. The intermediate $A^1\Sigma_u^+$ levels are perturbed by the $b^3\Pi_u$ Ω=0^+ state and "borrow" transition possibility from the $b^3\Pi_u$ Ω=0^+ state. The $b^3\Pi_u$ state has a spin-orbit constant, A≈200 cm^{-1} [13]. Since the $2^3\Delta_g$ and $b^3\Pi_u$ states have similar Hund's coupling schemes, the additional tran-

DOI:10.1063/1674-0068/26/01/13-19

sition selection rule is $\Delta\Sigma$=0. Thus, only transitions from $A^1\Sigma_u^+$-$b^3\Pi_{0u}$ mixed levels into $2^3\Delta_{1g}$ levels are allowed, and the $2^3\Delta_{1g}$←$A^1\Sigma_u^+$-$b^3\Pi_{0u}$ transition has P, Q, and R lines as expected. Other Ω components, $2^3\Delta_{2g}$ and $2^3\Delta_{3g}$, can only be observed via $A^1\Sigma_u^+$-$b^3\Pi_{1u}$ and $A^1\Sigma_u^+$-$b^3\Pi_{2u}$ mixed levels, respectively.

From Ref.[20, 21], the Fermi contact constants of the triplet Rydberg states in alkali dimers are close to 1/4 of the Fermi contact constant of the ground state of the alkali atom. For the Cs 6^2S state, $A_{\rm hf,atom}$=2298.16 MHz [22], where $A_{\rm hf,atom}$ is the atomic ^{2}S hyperfine parameter. Hence, the molecular parameter, $b_{\rm F}$≈574.5 MHz, where $b_{\rm F}$ is the Fermi-contact interaction constant for the alkali dimer Cs_2. To our knowledge, the Fermi-contact interaction is the most important part in the hyperfine splitting in the triplet Rydberg alkali dimers. Can the hyperfine structure be observed in the $2^3\Delta_{\rm g}$ state?

Qi *et al.* have analyzed the hyperfine structure of the Na_2 $2^3\Delta_{\rm g}$ state with a case a_β basis [23]. Here we use the same theory model and make a preliminary simulation of the hyperfine structure of the $2^3\Delta_{\rm g}$ state in Cs_2. The effective Hamiltonian for an isolated multiplet of a diatomic molecule is

$$\mathbf{H}^{\rm eff} = \mathbf{H}^{\rm rot} + \mathbf{H}^{\rm so} + \mathbf{H}^{\rm ss} + \mathbf{H}^{\rm sr} + \mathbf{H}^{\rm hfs} \tag{1}$$

The rotational and centrifugal distortion energies are given by,

$$\mathbf{H}^{\rm rot} = B_v\mathbf{R}^2 - D_v\mathbf{R}^4 \tag{2}$$

The spin-orbit interaction term is

$$\mathbf{H}^{\rm so} = A_v\mathrm{L}\cdot\mathbf{S} \tag{3}$$

The spin-spin interaction term is

$$\mathbf{H}^{\rm ss} = \frac{2}{3}\lambda(3\mathbf{S}_z^2 - \mathbf{S}^2) \tag{4}$$

And the spin-rotation interaction term is

$$\mathbf{H}^{\rm sr} = \gamma\mathbf{R}\cdot\mathbf{S} \tag{5}$$

The hyperfine interaction consists of three magnetic dipole terms:

$$\mathbf{H}^{\rm hfs} = \mathbf{H}^{\rm F} + \mathbf{H}^{\rm se} + \mathbf{H}^{\rm dip} + \mathbf{H}^{\rm higher\ multipoles} \tag{6}$$

where the Fermi-contact interaction is

$$\mathbf{H}^{\rm F} = b_{\rm F}\mathbf{I}\cdot\mathbf{S} \tag{7}$$

the nuclear spin-electron orbit interaction is,

$$\mathbf{H}^{\rm se} = a\mathbf{I}\cdot\mathbf{L} \tag{8}$$

and the dipolar interaction is

$$\mathbf{H}^{\rm dip} = \frac{1}{2}c(3\mathbf{I}_z\mathbf{S}_z - \mathbf{I}\cdot\mathbf{S}) \tag{9}$$

The term $\mathbf{H}^{\rm higher\ multipoles}$ stands for a contribution from higher multipoles. Due to the Rydberg character of the electronic states, the effects of the nuclear electric quadrupole interaction as well as other members of $\mathbf{H}^{\rm higher\ multipoles}$ are small and have been excluded in our calculation.

The parameters in the magnetic hyperfine Hamiltonian of Eqs. (7)−(9) are,

$$a = g_{\rm s}g_{\rm N}\mu_{\rm B}\mu_{\rm N}\sum_i\left\langle\frac{1}{r_i^3}\right\rangle_{av} \tag{10}$$

$$b_{\rm F} = \frac{8\pi}{3}g_{\rm s}g_{\rm N}\mu_{\rm B}\mu_{\rm N}\sum_i\left\langle\Psi_i^2(r_i=0)\right\rangle_{av} \tag{11}$$

$$c = \frac{3}{2}g_{\rm s}g_{\rm N}\mu_{\rm B}\mu_{\rm N}\sum_i\left\langle\frac{3\cos^2\theta_i - 1}{{r_i}^3}\right\rangle_{av} \tag{12}$$

Here $\mu_{\rm B}$ and $\mu_{\rm N}$ are the Bohr and nuclear magnetons, $g_{\rm s}$=2.0023 and $g_{\rm N}$ are the electron spin g-factor and nuclear spin g-factor, respectively. r_i and θ_i are the spherical polar coordinates of electron-i and defined with respect to the nucleus under consideration. The average is over the valence electrons.

The basis wave function in the case a_β coupling scheme is $|\Lambda S\Sigma J\Omega IF\rangle$. F is the total angular momentum quantum number including the nuclear spin. The molecular Hamiltonian matrix elements have been derived and more details can be found in Ref.[23]. All transitions are supposed to follow the Lorentzian function with full width at half maximum (FWHM) of about 45 MHz.

$$I(\omega-\omega_0) = I_0\frac{\Gamma^2}{(\omega-\omega_0)^2 + (\Gamma/2)^2} \tag{13}$$

where Γ is the FWHM and ω_0 is the transition frequency.

The calculations for hyperfine structures of the three Ω components of the $2^3\Delta_{\rm g}$ state with J=25 levels from the intermediate $A^1\Sigma_u^+$-$b^3\Pi_u$ state with J=24 levels are shown in Fig.4 (a)−(c). All three figures are set with the same energy scale. In Fig.4(a), transitions corresponding to different F components are shown in the simulation peak for the transition of $2^3\Delta_{1g}(J=25)$←$A^1\Sigma_u^+$-$b^3\Pi_{0u}(J'=24)$ and are compared with the experimental spectrum for the $2^3\Delta_{1g}(v=8,\ J=25)$←$A^1\Sigma_u^+(v'=7,\ J'=24)$ transition. Figure 4 (b) and (c) show the hyperfine splitting for transitions of $2^3\Delta_{2g}(J=25)$←$A^1\Sigma_u^+$-$b^3\Pi_{1u}(J'=24)$ and $2^3\Delta_{3g}(J=25)$←$A^1\Sigma_u^+$-$b^3\Pi_{2u}(J'=24)$, respectively. The calculation parameters are B_v=284.80 MHz, D_v=0.11 kHz, A_v=257.821 GHz, λ=0, γ=0, a=0 MHz, $b_{\rm F}$=574.55 MHz, and c=0 MHz. In Ref.[23], it has been proven that the rotational constants B_v and spin-orbit constants A_v are the most important ones besides the Fermi contact constant in case a_β coupling scheme. The values of rotational constants B_v and centrifugal distortion constant D_v are used from current Dunham fit in

DOI:10.1063/1674-0068/26/01/13-19

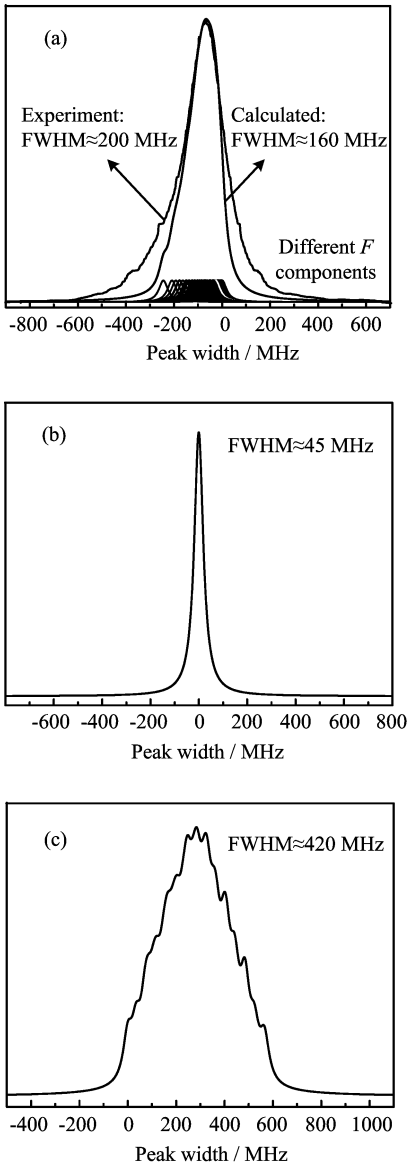

FIG. 4 Hyperfine structure calculations of the $2^3\Delta_g$ state (a) $2^3\Delta_{1g}(J{=}25){\leftarrow}A^1\Sigma_u^+{-}b^3\Pi_{0u}(J'{=}24)$ transition compared with the experimental observation $2^3\Delta_{1g}(v{=}8,\ J{=}25){\leftarrow}A^1\Sigma_u^+(v'{=}7,\ J'{=}24)$, (b) $2^3\Delta_{2g}(J{=}25){\leftarrow}A^1\Sigma_u^+{-}b^3\Pi_{1u}(J'{=}24)$ transition, (c) $2^3\Delta_{3g}(J{=}25){\leftarrow}A^1\Sigma_u^+{-}b^3\Pi_{2u}(J'{=}24)$ transition.

Table II. A_v and b_F are calculated from empirical formulas [6, 20, 21]. The spin-rotation constant γ, spin-spin constant λ and hyperfine constants a and c, which have little influence in our hyperfine simulations, can be set as 0.

From the calculations, the $\Omega{=}2$ component exhibits the smallest hyperfine splitting (FWHM≈45 MHz), while the FWHMs for peaks in $\Omega{=}1$ and 3 components are ∼160 and ∼420 MHz, respectively. Unlike the hyperfine splitting in the $3^3\Sigma_g^+$ state of Cs_2 which covers a total range of ∼10 GHz, the hyperfine splitting in the $2^3\Delta_g$ state of Cs_2 is much smaller. The reason lies in the different hyperfine coupling schemes. For the $3^3\Sigma_g^+$ state, it always belongs to the case $b_{\beta S}$ coupling scheme, while for the $2^3\Delta_g$ state in our observed range it can be described as a case a_β coupling scheme. The discussion on the hyperfine splitting of the $3^3\Sigma_g^+$ state will be published in a separate paper. Here, based on our calculations, we have a preliminary understanding of the hyperfine splitting pattern of the $2^3\Delta_g$ state. If mixed intermediate levels of $A^1\Sigma_u^+$-$b^3\Pi_{1u}$ and $A^1\Sigma_u^+$-$b^3\Pi_{2u}$ is determined experimentaly in the future, levels belonging to the $\Omega{=}2$ and 3 components of the $2^3\Delta_g$ state can be detected via two-step excitation techniques directly. It is possible that the hyperfine splitting might be resolved in the $2^3\Delta_{3g}$ levels, and at least, broadened peaks could be observed. On the contrary, a much sharper peak could be recorded in the transition from mixed intermediate levels of $A^1\Sigma_u^+$-$b^3\Pi_{1u}$ to $2^3\Delta_{2g}$ levels.

IV. CONCLUSION

The collision-induced energy transfer in the $A^1\Sigma_u^+$ state of Cs_2 has been observed and only rotational levels differing by $\Delta J{=}{\pm}2,\ {\pm}4,\ {\pm}6,\ \ldots,\ {\pm}2k$ from the parent level can be populated by collisions. 140 collisional lines from the intermediated state $A^1\Sigma_u^+$ into the $2^3\Delta_{1g}$ state of Cs_2 have been assigned based on the collision-induced energy transfer rules and accurate term values of the intermediate $A^1\Sigma_u^+$. Molecular constants and the RKR potential energy curve of the $2^3\Delta_{1g}$ state are recalculated including all experimental data available and can be used to get more accurate term values of the $2^3\Delta_{1g}$ state.

The different distribution patterns of collisional lines in P, Q, and R branches can be explained with the difference of rotational constants of the intermediate $A^1\Sigma_u^+$ state and upper $2^3\Delta_{1g}$ state. The hyperfine structure in the $2^3\Delta_{1g}$ state has been interpreted with a preliminary simulation based on a case a_β basis. The hyperfine splitting in the $2^3\Delta_{2g}$ is the smallest among three Ω components. The largest hyperfine splitting in the $2^3\Delta_{3g}$ is expected to be observed in a future experiment.

V. ACKNOWLEDGMENTS

This work was supported by the National Natural Science Foundation of China (No.11004117), the Foundation of Laboratory of Tsinghua University, and US National Science Foundation award PHY for Temple University (No.1205903). We are pleased to acknowledge fruitful discussions with Prof. J. Huennekens of Lehigh University and Dr. Jianbing Qi of Penn State Berks.

[1] C. Amiot and O. Dulieu, J. Chem. Phys. **117**, 5155 (2002).

DOI:10.1063/1674-0068/26/01/13-19

[2] J. A. Coxon and P. G. Hajigeorgiou, J. Chem. Phys. **132**, 094105 (2010).
[3] J. Bai, E. H. Ahmed, B. Beser, Y. Guan, S. Kotochigova, A. M. Lyyra, S. Ashman, C. M. Wolfe, J. Huennekens, F. Xie, D. Li, L. Li, M. Tamanis, R. Ferber, A. Drozdova, E. Pazyuk, A. V. Stolyarov, J. G. Danzl, H. C. Nägerl, N. Bouloufa, O. Dulieu, C. Amiot, H. Salami, and T. Bergeman, Phys. Rev. A **83**, 032514 (2011).
[4] D. Li, F. Xie, Li Li, S. Magnier, V. B. Sovkov, and V. S. Ivanov, Chem. Phys. Lett. **441**, 39 (2007).
[5] D. Li, F. Xie, and Li Li, Chem. Phys. Lett. **458**, 267 (2008).
[6] F. Xie, D. Li, L. Tyree, Li Li, V. B. Sovkov, V. S. Ivanov, S. Magnier, and A. M. Lyyra, J. Chem. Phys. **128**, 204313 (2008).
[7] F. Xie, V. B. Sovkov, A. M. Lyyra, D. Li, S. Ingram, J. Bai, V. S. Ivanov, S. Magnier, and L. Li, J. Chem. Phys. **130**, 051102 (2009).
[8] F. Xie, Li Li, D. Li, V. B. Sovkov, K. V. Minaev, V. S. Ivanov, A. M. Lyyra, and S. Magnier, J. Chem. Phys. **135**, 024303 (2011).
[9] Y. Chu, F. Xie, D. Li, Li Li, V. B. Sovkov, V. S. Ivanov, and A. M. Lyyra, J. Chem. Phys. **122**, 074302 (2005).
[10] F. Xie, D. Li, Li Li, R. W. Field, and S. Magnier, Chem. Phys. Lett. **431**, 267 (2006).
[11] D. Li, F. Xie, L. Li, V. B. Sovkov, V. S. Ivanov, E. Ahmed, A. M. Lyyra, J. Huennekens, and S. Magnier, J. Chem. Phys. **126**, 194314 (2007).
[12] S. Antonova, K. Urbanski, A. M. Lyyra, F. C. Spano, and L. Li, Chem. Phys. Lett. **267**, 158 (1997), and the references therein.
[13] N. Spies, Ph. D. thesis, *Fachbereich Chemie*, Kaiserslautern, Germany: University of Kaiserslautern, (1989).
[14] H. Weickenmeier, U. Diemer, M. Wahl, M. Raab, W. Demtröder, and W. Müller, J. Chem. Phys. **82**, 5354 (1985).
[15] H. Weickenmeier, U. Diemer, W. Demtröder, and M. Broyer, Chem. Phys. Lett. **124**, 470 (1986).
[16] S. Sainis, *Ph. D. Thesis*, New Haven, USA: Yale University, (2005).
[17] T. Kobayashi, T. Usui, T. Kumauchi, M. Baba, K. Ishikawa, and H. Katô, J. Chem. Phys. **98**, 2670 (1993).
[18] S. Kasahara, Y. Hasui, K. Otsuka, M. Baba, W. Demtröder, and H. Katô, J. Chem. Phys. **106**, 4869 (1997).
[19] S. Kasahara, K. Otsuka, M. Baba, and H. Katô, J. Chem. Phys. **109**, 3393 (1998).
[20] L. Li, Q. Zhu, and R. W. Field, J. Mol. Spectrosc. **134**, 50 (1989).
[21] H. Katô, M. Otani, and M. Baba, J. Chem. Phys. **91**, 5124 (1989).
[22] E. Arimondo, M. Inguscio, and P. Violino, Rev. Mod. Phys. **49**, 31 (1977).
[23] P. Qi, G. Lazarov, A. M. Lyyra, Y. Liu, C. Cui, L. Li, and G. H. Jeung, J. Chem. Phys. **124**, 184304 (2006).

DOI:10.1063/1674-0068/26/01/13-19